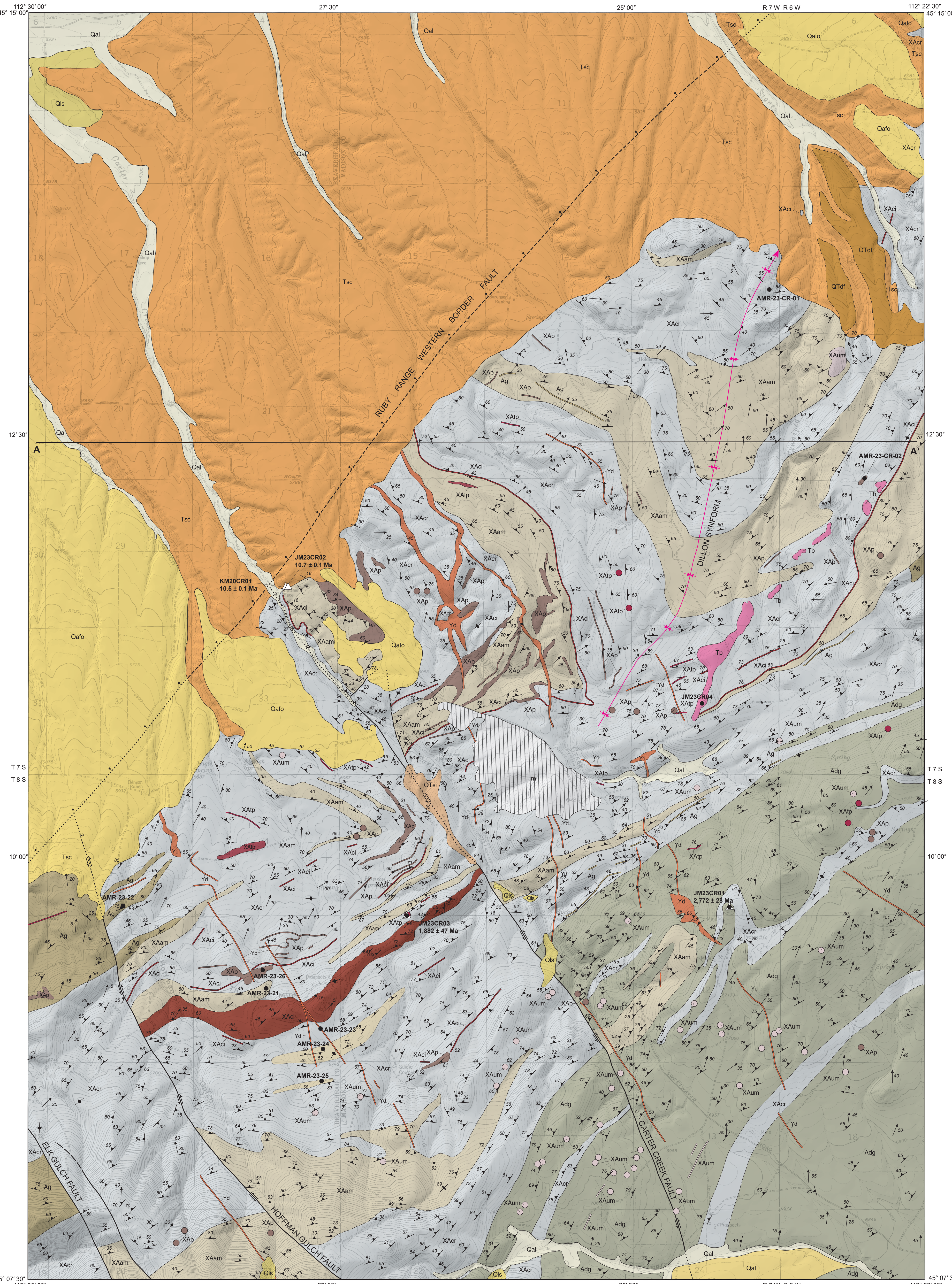

Base map produced by the United States Geological Survey
Christensen Ranch 1:24,000-scale quadrangle map
Control by: USGS and USC&GC
Compiled from aerial photographs taken 1960
Field checked: 1961
Projection: Polyconic
Vertical Datum: National Geodetic Vertical Datum of 1929
Horizontal Datum: 1927 North American Datum

Shaded relief created from 10-meter digital elevation model from U.S. Geological Survey National Elevation Dataset.

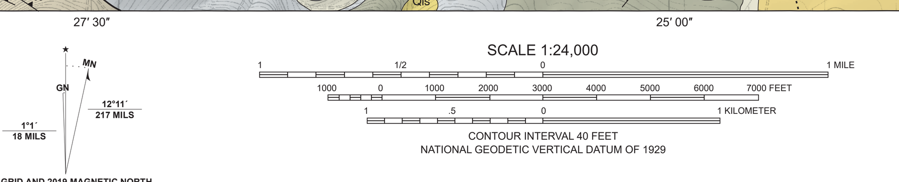

Maps may be obtained from:
Publications Office
Montana Bureau of Mines and Geology
1300 West Park Street
Butte, Montana 59701-8997
Phone: (406) 496-4174
https://mbmg.mtech.edu

CORRELATION CHART

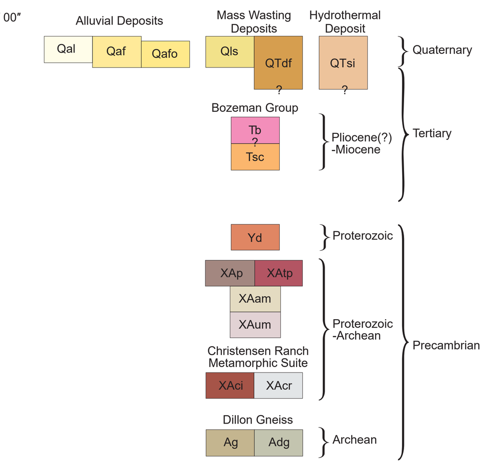

MAP SYMBOLS

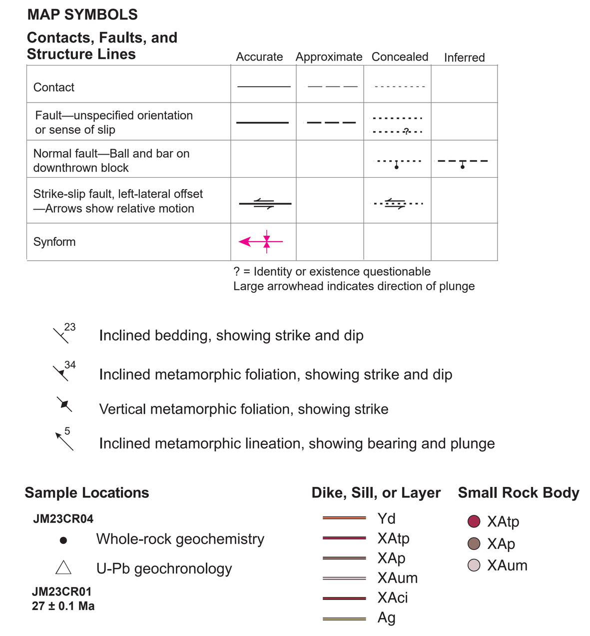

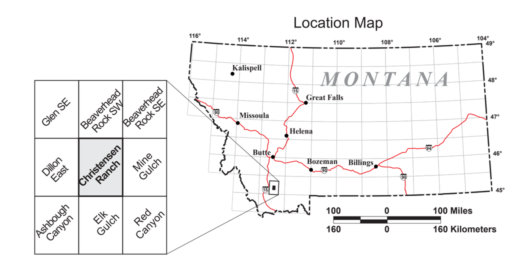

Cross Section A–A′

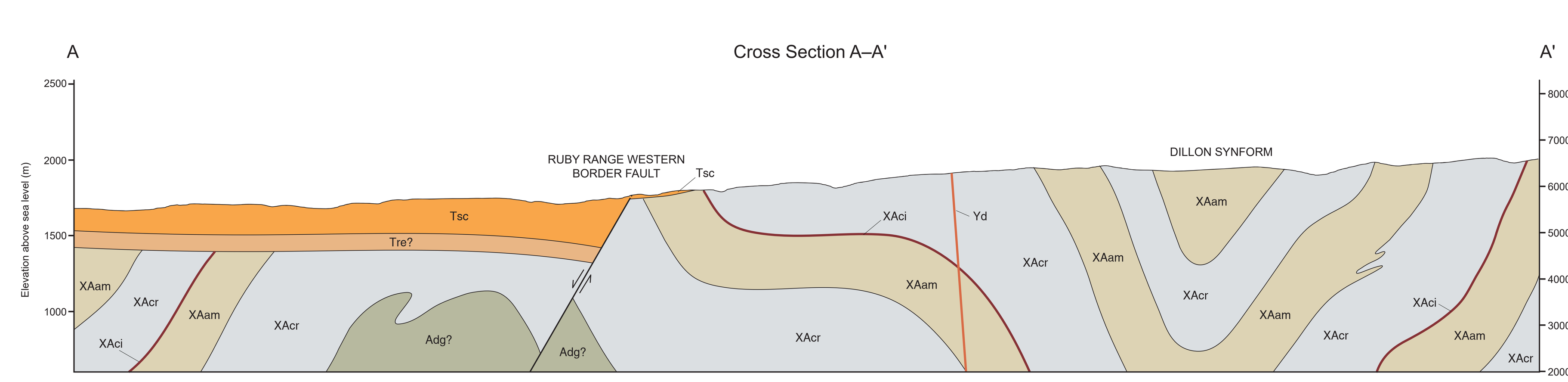

No vertical exaggeration
Surficial units not shown

Unit not exposed in map area but shown in cross-section:

Tre — Renova Formation (Bozeman Group)

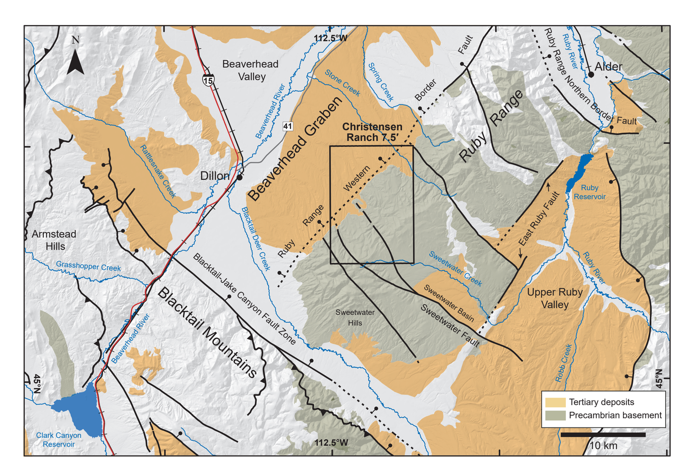

Figure 1. Location and physiographic setting of the map area. Geologic elements were modified from Ruppel and others (1993), Vuke and others (2007), and mapping in this study.

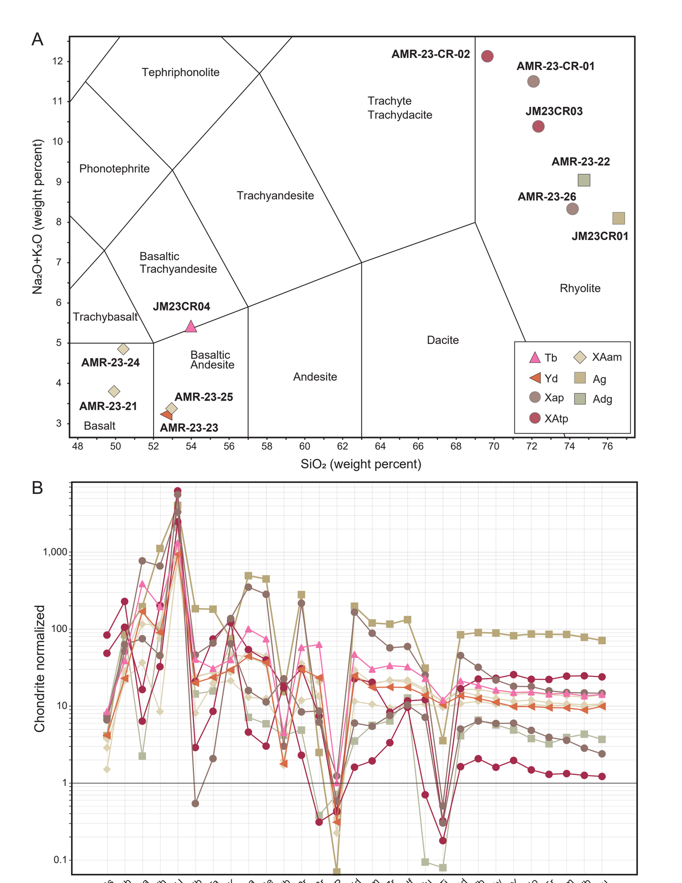

Figure 2. Whole-rock geochemical data. (A) Total alkali silica classification diagram of normalized values after Le Bas and others (1986). (B) Chondrite-normalized rare earth element plot after Sun and McDonough (1989). Data are color coded by formation; plots share the legend in (A).

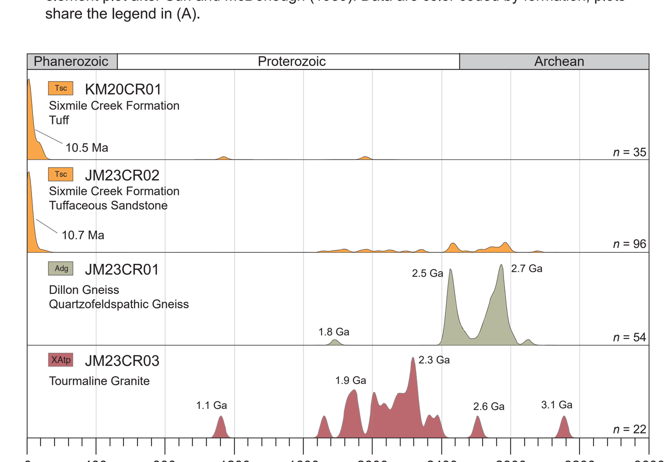

Figure 3. Kernel density estimate (KDE) plots of the ^{207}Pb corrected $^{206}Pb/^{238}U$ (<1,400 Ma) and $^{207}Pb/^{206}Pb$ (>1,400 Ma) zircon age data. KDE bandwidths and bin widths are 20 m.y. A 20 percent discordance filter was applied to the data. Significant peaks and maximum depositional ages are labeled.

LOCATION AND PHYSIOGRAPHIC SETTING

The Christensen Ranch 7.5′ quadrangle is located in Beaverhead and Madison Counties, approximately 16 km (10 mi) east–southeast of Dillon, Montana. The map area covers parts of the Sweetwater Hills and Beaverhead Valley near the southern terminus of the Ruby Range (fig. 1). The Sweetwater Hills are characterized by hilly and rugged upland terrain covered by a mix of grassland and sagebrush steppes, with some tracts of coniferous woodlands. The exposure of the bedrock geology and overlying unconsolidated Tertiary–Quaternary deposits is generally good to excellent. The map area spans a drainage divide separating Sweetwater and Stone creeks, which flow to the Jefferson River basin. Elevations range from 1,765 m (5,790 ft) along Blacktail Deer Creek to 2,588 m (8,490 ft) at Benson Peak.

PREVIOUS MAPPING

The Christensen Ranch 7.5′ quadrangle is covered by small-scale mapping by Ruppel and others (1993, scale 1:250,000) and Klepper (1950, scale 1:250,000). Large-scale mapping by Okuma (1971, scale 1:24,000) and James (1990, scale 1:24,000) covered the southeast part of the quadrangle and was focused on the metamorphic rocks. Petrological and mapping studies of the Precambrian basement rocks outside the Christensen Ranch quadrangle were done by Garihan (1979a,b), Karasevich (1980), Dahl (1979, 1980), Dahl and Friberg (1980), and Desmarais (1981). The region's Tertiary stratigraphic framework is summarized by Thomas and Sears (2020), Vuke (2020), and references therein.

METHODS

Geologic Mapping

Field mapping was conducted over approximately 3.5 months in 2023 for the STATEMAP component of the United States Geological Survey (USGS) National Cooperative Geologic Mapping Program (NCGMP). A 1:24,000-scale topographic base was utilized for field mapping, and geologic contacts were refined using high-resolution satellite imagery (ESRI, 2024) and 2024 USGS 3DEP lidar data. Structure and observational data were located and measured with a traditional hand transit and an Apple iPhone 14. Additional data were compiled from James (1990). Metamorphic foliations represent all types of recognizable surfaces of metamorphic origin. In gneiss and metasedimentary rocks, the foliation commonly parallels mineral compositional layering. Metamorphic lineations represent mineral alignment, fold axes, and the intersection of foliation planes. Igneous foliations are surfaces formed by mineral alignment in the groundmass. Field sheets were scanned and georegistered in GIS software. The geologic data were subsequently digitized to the Geologic Map Schema (GeMS) geodatabase required by the NCGMP. Structure data and geologic contacts were compiled from Okuma (1971) and James (1990).

Whole-Rock Element Chemistry and U-Pb Geochronology

Rock samples for whole-rock geochemistry and U-Pb geochronology were processed at the MBMG mineral separation laboratory. A 100- to 200-g split of the crushed material was prepared for bulk-rock geochemical analysis and analyzed by X-ray fluorescence (XRF) and inductively coupled plasma mass spectrometry at the Peter Hooper GeoAnalytical Lab, Washington State University. Zircon was isolated from rock and sediment samples using standard density and magnetic separation techniques at the MBMG mineral separation laboratory and analyzed by laser ablation inductively coupled plasma mass spectrometry (LA-ICPMS) at the University of California, Santa Barbara.

Bulk-rock major and trace element geochemical data are plotted in figure 2 (see Mosolf and others, in review). U-Pb age spectra are plotted in figure 3 and interpretative ages are provided in table 1. The complete U-Pb zircon datasets and analytical methods are reported in Mosolf and others (2023) and Brennan and others (2025).

DESCRIPTION OF THE MAP UNITS

The Christensen Ranch geologic map shows rock units exposed at the surface or overlain by thin surficial deposits. Surficial sedimentary and mass movement deposits are shown where they are thick and extensive enough to be mapped at 1:24,000 scale. Igneous and metamorphic rocks are classified using the International Union of Geological Sciences nomenclature (Le Bas and Streckeisen, 1991; Schmid and others, 2007). Minerals in igneous and metamorphic rock units are listed in order of decreasing abundance. Grain size classification of unconsolidated and consolidated sediment is based on the Wentworth scale (Lane, 1947). Multiple lithologies within a rock unit are listed in order of decreasing abundance.

Quaternary–Tertiary Sedimentary Deposits

Older Quaternary alluvial fans (Qafo) and debris flow deposits (QTdf) rest on poorly consolidated Tertiary sedimentary deposits along the western range front. Siliceous hydrothermal deposits (QTsi) coincide with the Carter Creek fault, possibly postdating fault movement. Extensive alluvial stream deposits (Qal) have formed in stream catchments in the Sweetwater Hills, including Hoffman, Carter, Bachelor, and Stone creeks. Small landslide deposits (Qls) occur throughout the map area. A substantial open cut pit and associated tailings (m) associated with the Regal Mine occur along the Sweetwater Road in the central part of the map area; talc mining was active at the time of this study.

m — **Land modified by mining**—Land disturbed by open-cut talc mine and associated tailings.

Qal — **Alluvium (Quaternary: Holocene)**—Unconsolidated, poorly sorted cobbles, gravel, sand, and silt along Stone Creek and tributary drainages. Thickness as much as 10 m (33 ft).

Qaf — **Alluvial fan deposit (Quaternary: Holocene and Pleistocene?)**—Unconsolidated, poorly sorted cobbles, gravel, sand, and silt forming a fan-shaped deposit in the southern part of the map area. Thickness as much as 30 m (100 ft).

Qls — **Landslide deposit (Quaternary: Holocene and Pleistocene?)**—Unstratified, poorly sorted rock fragments deposited by slumps, slides, rock falls, and debris flows. Typically characterized by hummocky topography, subdued landslide scarps, and rock talus. Variable thickness, generally less than 30 m (100 ft).

Qafo — **Alluvial fan deposit, older (Pleistocene)**—Unconsolidated, poorly sorted, cobbles, gravel, sand, and silt forming broad incised surfaces along the range front above the level of modern streams. Deposited as coalescent alluvial fan channels and debris flow fans. Variable thickness, with a maximum of at least 10 m (30 ft).

QTdf — **Debris-flow deposit (Pleistocene? and Miocene?)**—Poorly sorted gravel and sand with angular to subrounded cobbles and boulders up to 3 m (10 ft) in length. Clasts are predominantly Archean crystalline basement rock. Interpreted to be debris flow deposits formed on a slope dipping gently to the northwest away from the range front. Thickness up to 10 m (30 ft).

QTsi — **Siliceous hydrothermal deposits (Quaternary and Pliocene?)**—Brown masses of jasperoid up to 400 m (1,300 ft) wide coinciding with the Carter Creek fault zone.

Tertiary Volcano-Sedimentary Deposits

Tertiary sedimentary deposits of the Sixmile Creek Formation (Bozeman Group) were mapped on the northwest flank of the Sweetwater Hills, unconformably overlying the Archean basement rocks and cut by the Ruby Range western border fault. The poorly lithified deposits generally consist of interbedded tuffaceous sandstone and conglomerate beds (fig. 4A; Thomas and Sears, 2020). Scattered outcroppings of basalt in the northern part of the quadrangle (Tb) are possibly equivalent to the Timber Hill Basalt member (approximately 6 Ma; Fritz and others, 2007), or a Pliocene basalt northeast of the map area (approximately 4 Ma; Marvin and others, 1974).

Tb — **Basalt, undivided (Miocene to Pliocene?)**—Small outcroppings of aphanitic basalt containing sparse olivine phenocrysts (<1 percent). Occurs as scattered outcrops in the northern half of the quadrangle. Thickness unknown.

Tsc — **Sixmile Creek Formation (Miocene to Pliocene?)**—Pale orange to gray, poorly consolidated, interbedded tuffaceous to quartz-rich silt, sand, gravel, and conglomerate. Conglomerate intervals are poorly sorted, massive to cross-bedded, clast- to matrix-supported with cobbles and boulders mostly derived from Archean basement rocks. Poorly lithified intervals consist of thin- to thick-bedded, massive to cross-stratified silt, sand, and gravel with occasional tuff interbeds. The unit is locally calcareous along the trace of the Ruby Range western border fault. The base is not exposed but estimated to be up to 305 m (1,000 ft) thick. A tuffaceous sequence near Guntner Place (section 28, T. 7 S., R 7 W.) yielded U-Pb zircon max depositional ages of 10.7 ± 0.1 Ma and 10.5 ± 0.1 Ma (table 1).

Precambrian Metamorphic and Intrusive Rocks

The Ruby Range is underlain by three belts of Precambrian metamorphic rock, including the Elk Gulch Suite, the Dillon Gneiss, and the Christensen Ranch Metasedimentary Suite. The Elk Gulch Suite is not exposed in the map area, but is assumed to be the structurally deepest metamorphic assemblage in the region, consisting of gneiss, migmatite, and amphibolite. Minimum emplacement ages of gneissic intervals span approximately 2.79–2.72 Ga in the south-adjacent Elk Gulch quadrangle (Mosolf, 2025). The Dillon Gneiss (Adg) forms the crest of the Ruby Range and is mostly massive-to-foliated granitic gneiss with subordinate amphibolite and metasedimentary intercalations. The gneissic sequences are enriched in incompatible elements with minimum emplacement ages of 2.8–2.5 Ga (figs. 2, 3; Mosolf, 2025). The Elk Gulch Suite and Dillon Gneiss are difficult to differentiate in the field; the former tends to be more mafic and richer in plagioclase (Garihan, 1979b). The Christensen Ranch Metasedimentary Suite (XAcr; fig. 4B) is a complex sequence of metasedimentary rock distinguished by intertonguing marble and schist intervals assumed to be younger than the Elk Gulch Suite and Dillon Gneiss (James, 1990). Complexly deformed iron formation (XAci; fig. 4C) occurs at several structural levels in the metasedimentary sequence. Amphibolite (XAam) screens and sheets are interleaved throughout the basement assemblages but are only mapped in areas thick enough to be shown at 1:24,000 scale. Pegmatite (XAp and XAtp) and ultramafic rock (XAum) intrude the older Precambrian rocks locally. Northwest-striking diabase dikes generally crosscut the basement metamorphic fabrics and parallel northwest-striking fractures and faults.

Yd — **Diabase (Mesoproterozoic?)**—Diabase dikes are approximately 1–30 m (3–100 ft) thick with continuous lengths exceeding 8.5 km (5.3 mi). Diabase is recessive and weathers to spheroidal boulders, commonly creating topographic sags. The rock is frequently altered to secondary minerals, but original diabasic and gabbroic textures are well preserved. Primary minerals appear to have been plagioclase and pyroxene, with minor amounts of quartz, magnetite, and ilmenite. Secondary minerals include actinolite, chlorite, and sericite. Wooden and others (1978) described the diabase in the Ruby Range as low potassium tholeiite with a whole-rock Rb-Sr age of 1.4 Ga.

XAtp — **Tourmaline granite (Early Proterozoic (?) or Late Archean(?))**—Small bodies of undeformed pegmatite up to 65 m (200 ft) wide consisting of interlocking grains of perthitic microcline, twinned plagioclase (oligoclase–albite), and quartz, and variable amounts of diagnostic tourmaline. Pegmatite bodies are commonly zoned with a rose quartz core. Locally crosscut by diabase dikes (James, 1990; Wooden and others, 1978). U-Pb zircon dating yielded a complex age spectrum with a maximum emplacement age of approximately 1.88 Ga, and a single crystal date of 1.12 Ga (fig. 3).

XAp — **Pegmatite sheets and dikes (Early Proterozoic (?) or Late Archean(?))**—Pegmatite sheets and dikes up to tens of meters wide with continuous lengths exceeding 1 km (0.6 mi). Typically consist of coarse-grained alkali feldspar and quartz with minor amounts of albite–oligoclase and rare muscovite, tourmaline, and garnet. Most bodies show cataclastic deformation and are locally foliated parallel to the country rock. Dike swarms were mapped as bodies over 300 m (984 ft) wide and 3 km (1.9 mi) long.

XAam — **Amphibolite (Archean or Early Proterozoic)**—Black and white, massive- to well-foliated, sheet-like bodies primarily composed of fine- to coarse-grained hornblende, plagioclase, and quartz. Amphibolite occurs as two compositional varieties: gneiss containing 40–50 percent hornblende in alternating hornblende-rich and quartz–plagioclase-rich layers; or hornblendite with accessory plagioclase and quartz. The presence of garnet varies locally from approximately 0 to 25 percent. Amphibolite is intercalated with the other basement assemblages, ranging in size from centimeter-scale lenses to sheets tens of meters thick.

XAum — **Ultramafic rocks (Late Archean or Early Proterozoic)**—Intrusive pods or lenses of ultramafic rock up to tens of meters wide (Heinrich, 1960, 1963). Ultramafic rock is dark green or black, fine- to coarse-grained, and primarily massive to schistose. Weathering surfaces are commonly studded with resistant poikilitic orthopyroxene grains up to a few centimeters in diameter. Protolith rocks likely ranged from harzburgite to pyroxenite, but most occurrences have been modified extensively by serpentinization and post-emplacement metamorphism.

XAci — **Iron formation, Christensen Ranch Metasedimentary Suite (Early Proterozoic or Late Archean)**—Black to dark gray iron formation that creates resistant ridges locally but more commonly weathers to recessive, reddish brown soils. Typically occurs as a dark, high-density rock composed of layered magnetite and quartz that is commonly discontinuous and complexly folded. Beds range in thickness from less than 0.3 m (1 ft) up to 10 m (33 ft) thick and are commonly intercalated with mica schist and quartzite but can also be found within dolomitic marble. Layered structure gives the unit a streaky or gneissic appearance. Occurs at multiple structural levels throughout the Christensen Ranch Metasedimentary Suite. The structural thickness exceeds 400 m (1,300 ft).

XAcr — **Christensen Ranch Metasedimentary Suite, undivided (Early Proterozoic or Late Archean)**—A complex sequence of marble, schist, and quartzite that is intercalated with gneiss and amphibolite. Variable exposure made delineating the metasedimentary units challenging at 1:24,000 scale; therefore, the metasediments were mapped as a single unit (XAcr). See James (1990) and Okuma (1971) for detailed mapping of the subunits. Previous U-Pb monazite dating of schist, amphibolite, and gneiss yielded peak metamorphic ages spanning approximately 1.81–1.75 Ga (Jones, 2008; Cramer, 2015).

Undifferentiated metasedimentary rocks (Late Archean or Early Proterozoic)—Complex assemblage of quartz–mica schist and quartzose gneiss; calc–silicate gneiss and schist; and anthophyllite schist locally intercalated with amphibolite and quartzite. Generally recessive and not well exposed throughout the map area. Thickness unknown.

Marble (Late Archean to Early Proterozoic)—White, gray, orange-brown, medium to coarsely crystalline dolomitic and calcitic marble that forms outcrops commonly covered with bright orange lichen. Contains light-colored diopside, tremolite, and scarce graphite; conspicuous dark green blebs of serpentine and phlogopite are characteristic of some intervals. Marble forms massive- to well-foliated successions that appear conformable; however, the original stratigraphic order has likely been disrupted by bedding-plane faults and possible nappe development. In the southern part of the map area, marble layers are isoclinally folded into the older gneissic assemblages. Thicker intervals of pure marble are dominantly dolomitic in composition and commonly host talc deposits occurring as seams and pods. Structural thickness exceeds 400 m (1,313 ft).

Ag — **Granite Gneiss (Late Archean)**—Brown, medium-grained, moderately well-foliated rock composed of finely perthitic microcline, plagioclase, and quartz, with lesser biotite and green hornblende. Accessory minerals include apatite, allanite, magnetite, zircon, and garnet. The granite gneiss appears to be developed in or engulfing quartzite-bearing strata along the range front in the southwest part of the map area. Locally, the rock is strongly sheared and mylonitic, otherwise physically indistinguishable from older quartzofeldspathic gneisses. The age of the gneiss is not constrained but is considered age equivalent to the other gneiss units (James, 1990). Thickness unknown.

Adg — **Dillon Gneiss (Archean)**—Gray to reddish brown, massive- to well-foliated, medium- to coarse-grained, locally garnetiferous gneiss of granitic composition that typically forms large, rounded outcrops. Potassium feldspar is the most abundant mineral, intergrown with oligoclase and quartz in nearly equal proportions. Subordinate mineral constituents include biotite, muscovite, garnet, and fibrous sillimanite. Massive to weakly foliated gneiss often grades into a strongly banded gneiss with a greater abundance of darker minerals, including biotite, garnet, and occasional hornblende. The Dillon Gneiss includes subordinate layers and pods of amphibolite, narrow ribbons of infolded marble, thin layers of pelitic gneisses and schists, and ultramafic rock. Originally named the "Dillon Granite Gneiss" (Heinrich, 1960) and subsequently referred to as "Quartzofeldspathic Gneiss" by James (1990). Stotter (2019) suggested the assemblage be renamed the "Dillon Gneiss," which is the name adopted on this map. U-Pb zircon dating yielded a minimum emplacement age of approximately 2.74 Ga (fig. 3, table 1) in the map area.

STRUCTURAL GEOLOGY

Precambrian Deformation

A penetrative foliation is generally parallel to compositional and migmatic layering (fig. 5A), and appears to be penetrative across the Dillon Gneiss and Christensen Ranch Metasedimentary Suite assemblages. Prevalent isoclinal folding is generally axial planar to the main metamorphic foliation and plunges northeasterly, paralleling mineral and intersection lineations (fig. 5B). Early folding and the primary metamorphic foliation were subsequently deformed by at least two generations of folds, including the map-scale Dillon synform. Several northwest-trending fault systems transect the quadrangle, comprising the Hoffman Gulch and Carter Creek faults. Both were active in Precambrian time with left-lateral displacements up to 1.3 km (0.8 mi). Shearing and mylonization of Archean granitic gneiss (Ag) records tectonic deformation as early as 2.7 Ga (James, 1990). Weakly deformed pegmatite (XAp and XAtp) suggests early Precambrian deformation continued in the Early Proterozoic(?). Diabase dikes (Yd) generally crosscut the older deformational fabrics and structures, constraining early Precambrian deformation and metamorphism before approximately 1.7–1.4 Ga. Previously published geochronology ages (e.g., Jones, 2008; Cramer, 2015; Harms and Baldwin, 2020) and U-Pb zircon data from this study (fig. 3) generally support field relationships, recording magmatic and tectonothermal activity ca. 2.8–2.7 Ga; 2.5–2.4 Ga (Beaverhead/Tendoy orogeny); and 1.8–1.7 Ga (Big Sky orogeny).

Cordilleran Thrust Belt Deformation

Paleozoic–Mesozoic strata that unconformably rest on the crystalline basement in the northern Ruby Range were deformed by Late Cretaceous folds and faults (Tysdal, 1976; Gavillot and others, 2024; Parker and Gavillot, 2024). In the southern part of the range, the Phanerozoic cover was exhumed and completely eroded during crustal shortening, exposing the Precambrian basement rocks in the Christensen Ranch quadrangle. Cordilleran structures were not readily identified in the map area, but the older northwest-striking Precambrian faults were possibly reactivated as contractional structures during crustal shortening. Low-temperature thermochronology data from the northern part of the Ruby Range suggest that rapid cooling and inferred tectonic exhumation of the basement rocks were underway by approximately 80 Ma (Carrapa and others, 2019).

Cenozoic Extensional Deformation

Northwest-trending faults break the Ruby Range into structural blocks that have a prolonged deformational history spanning the Precambrian to Cenozoic (Schmidt and Garihan, 1983; James, 1990). Several of the faults were extensionally reactivated in the Ruby Range during Tertiary time and have remained active to the Quaternary (e.g., Stickney and Bartholomew, 1987). Extensive hydrothermal silicification has occurred along the Carter Creek fault during or after Tertiary–Quaternary movement on the fault. The Hoffman Gulch and Carter Creek faults appear structurally linked to the Sweetwater fault (Mosolf and Sears, 2024), which is assumed to be Quaternary-active with a poorly constrained fault slip rate of approximately 0.03–0.04 mm/yr (0.001–0.002 in/yr; Stickney and Bartholomew, 1987; Ostenaa and Wood, 1990; Fritz and Sears, 1993).

The northeast-striking Ruby Range western border fault was previously mapped as a 24-mi-long (38 km) Quaternary fault with a poorly constrained slip estimate of <0.2 mm/yr, similar to other seismogenic faults in southwest Montana (Stickney and others, 2000). The basement rocks appear truncated by the fault but clear evidence of Quaternary displacement along the range front is not readily observable. Deep incision and a lack of fault scarps formed in the Tertiary–Quaternary sedimentary deposits onlapping the fault suggest that little displacement has occurred in the past 130,000 years (this map; Gavillot and others, 2024). Fault intersections are concealed by the Tertiary–Quaternary cover, but recent seismicity immediately outside the quadrangle (M 4.1, 2024) suggests strike-slip movement has continued on the northwest-trending faults, post-dating the Ruby Range western border fault.

TALC DEPOSITS

Talc deposits occur throughout the map area and have been mined sporadically for decades (Berg, 1979). Talc and associated chlorite formed through hydrothermally driven, constant-volume replacement of the dolomitic marbles in the Christensen Ranch Suite (XAcr; Underwood and others, 2014). Talc is generally cryptocrystalline, varying from opaque to translucent, and its color ranges from white to pale green or olive gray (James, 1990). Its contact with the country rock is typically sharp, forming elongated bodies that parallel foliation planes. The Regal Mine, formerly known as the Keystone Mine, is the site of the largest talc body in the map area and was actively mined as an open pit at the time of this report. The Regal orebody is up to 60 m (200 ft) thick and dips 30–75° northward near the axis of a tightly refolded synform. A steeply dipping, northwest-trending brecciated fault zone bounds the eastern extent of the main ore body (Berg, 1979). A near-vertical Proterozoic diabase dike (Yd) 18–30 m (60–100 ft) thick is exposed near the western end of the deposit and is the inferred heat source for the hydrothermal cells that produced the orebody (Underwood and others, 2014).

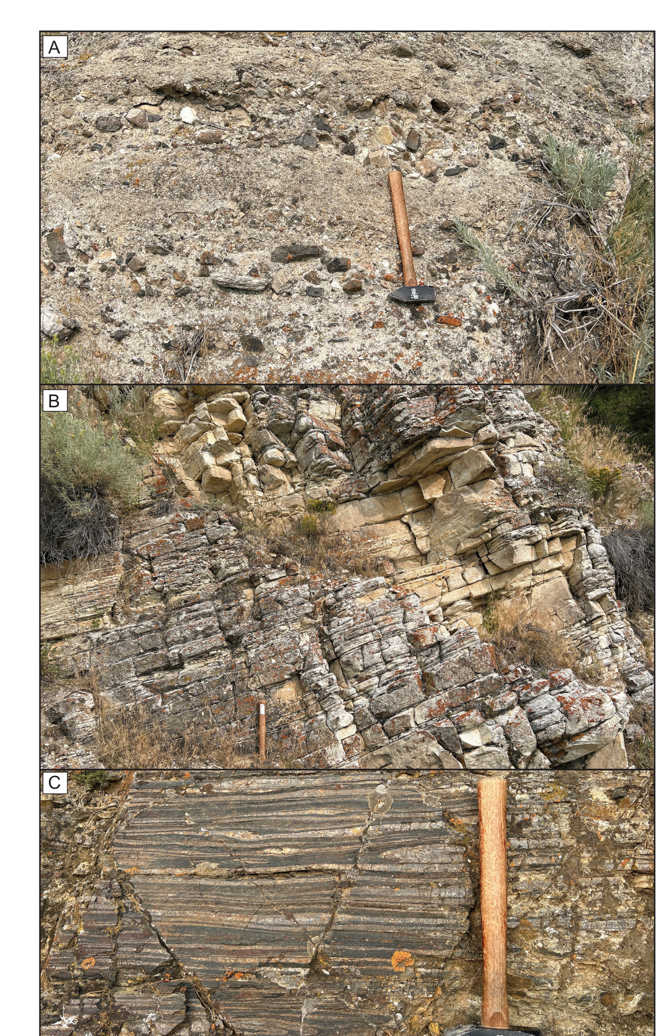

Figure 4. (A) Interbedded gravel and tuffaceous sandstone of the Tertiary Sixmile Creek Formation (Tsc) exposed in the Carter Creek drainage. (B) Layered and foliated dolomitic marble of the Christensen Ranch Suite (XAcr). (C) Banded and folded quartzite and iron formation (XAci). Rock hammer for scale.

REFERENCES

Berg, R.B., 1979, Talc and chlorite deposits in Montana: Montana Bureau of Mines and Geology Memoir 45, 66 p., 3 sheets.
Brennan, D.T., Parker, S., Mosolf, J.G., and Kylander-Clark, A., 2025, U-Pb geochronology data from rock samples collected in western Montana, 2023–2024: Montana Bureau of Mines and Geology Analytical Dataset 16.
Carrapa, B., DeCelles, P.G., and Romero, M., 2019, Early inception of the Laramide orogeny in southwestern Montana and northern Wyoming: Implications for models of flat-slab subduction: Journal of Geophysical Research: Solid Earth, v. 124, p. 2102–2123.
Cramer, M., 2015, Proterozoic tectonometamorphic evolution of the Ruby Range, SW Montana, USA: Insights from phase equilibria modeling and *in situ* monazite petrochronology: Missoula, University of Montana, M.S. thesis, 120 p.
Dahl, P.S., 1979, Comparative geothermometry based on major-element and oxygen isotope distributions in Precambrian metamorphic rocks from southwestern Montana: American Mineralogist, v. 64, p. 1280–1293.
Dahl, P.S., 1980, The thermal-compositional dependence of Fe^{2+}-Mg distributions between coexisting garnet and pyroxene-applications to geothermometry: American Mineralogist, v. 65, p. 854–866.
Dahl, P.S., and Friberg, L.M., 1980, The occurrence and chemistry of epidote-clinozoisites in mafic gneisses from the Ruby Range, southwestern Montana: University of Wyoming Contributions to Geology, v. 18, no. 2, p. 77–82.
Desmarais, N.R., 1981, Metamorphosed Precambrian ultramafic rocks in the Ruby Range, Montana: Precambrian Research, v. 16, p. 67–101.
ESRI, 2024, "World_Imagery" [basemap], scale not given, available at: https://services.arcgisonline.com/ArcGIS/rest/services/World_Imagery/MapServer. [Accessed June 17th, 2024].
Fritz, W.J., and Sears, J.W., 1993, Tectonics of the Yellowstone hotspot wake in southwestern Montana: Geology, v. 21, p. 427–430.
Fritz, W.J., Sears, J.W., McDowell, R.J., and Wampler, J.M., 2007, Cenozoic volcanic rocks of southwestern Montana: Northwest Geology, v. 36, p. 91–110.
Garihan, J.M., 1979a, Geology and structure of the central Ruby Range, Madison County, Montana Summary: Geological Society of America Bulletin, Part I, v. 90, no. 4, p. 323–326.
Garihan, J.M., 1979b, Geology and structure of the central Ruby Range, Madison County, Montana: Geological Society of America Bulletin, Part II, v. 90, p. 695–788.
Gavillot, Y.G., Parker, S.D., and Pearson, D.M., 2024, Geologic map of the Beaverhead Rock SE 7.5′ quadrangle, Madison county, Montana: Montana Bureau of Mines and Geology Geologic Map 101, 1 sheet, scale 1:24,000.
Harms, T.A., and Baldwin, J.A., 2020, Paleoproterozoic geology of Montana, in Metesh, J.J., and Vuke, S., eds.: Montana Bureau of Mines and Geology Special Publication 122: Geology of Montana—Geologic History, v. 1, 65 p., available at http://www.mbmg.mtech.edu/pubs/GeologyofMontana/
Heinrich, E.W., 1960, Geology of the Ruby Mountains and nearby areas in southwestern Montana, *in* Pre-Beltian geology of the Cherry Creek and Ruby Mountains areas, southwestern Montana: Montana Bureau of Mines and Geology Memoir 38, p. 31–62.
Heinrich, E.W., 1963, Paragenesis of clinohumite and associated minerals from Wolf Creek, Montana: American Mineralogist, v. 48, p. 597–613.
James, H.L., 1990, Precambrian geology and bedded iron deposits of the southwestern Ruby Range, Montana: U.S. Geological Survey Professional Paper 1495, p. 1–39.
Jones, C.L., 2008, U-Pb geochronology of monazite and zircon in Precambrian metamorphic rocks from the Ruby Range, SW Montana: Deciphering geological events that shaped the NW Wyoming province: Kent, Kent State University, M.S. thesis, 119 p.
Karasevich, L.P., 1980, Structure of the pre-Beltian metamorphic rocks of the northern Ruby Range, southwestern Montana: Harrisburg, Pennsylvania State University, M.S. thesis, 172 p.
Klepper, M.R., 1950, Geologic reconnaissance of parts of Beaverhead and Madison counties, Montana: U.S. Geological Survey Bulletin 969-C, p. 55–85, scale 1:250,000.
Lane, E.W., 1947, Report of the subcommittee on sediment terminology: Transactions of the American Geophysical Union, v. 28, no. 6, p. 936–938.
Le Bas, M.J., and Streckeisen, A.L., 1991, The IUGS systematics of igneous rocks: Journal of the Geological Society of London, v. 148, p. 825–833.
Le Bas, M.J., LeMaitre, R.W., Streckeisen, A., and Zanettin, B., 1986, A chemical classification of volcanic rocks based on the total alkali silica diagram: Journal of Petrology, v. 27, p. 745–750.
Marvin, R.F., Wier, K.L., Mehnert, H.H., and Merritt, V., 1974, K-Ar ages of selected Tertiary igneous rocks in southwestern Montana: Isochron/West, v. 10, p. 17–20.
Mosolf, J.G., 2025, Geologic map of the Elk Gulch 7.5′ quadrangle, Beaverhead and Madison counties, Montana: Montana Bureau of Mines and Geology Geologic Map 108, 1 sheet, scale 1:24,000.
Mosolf, J.G., and Kylander-Clark, A., 2023, U-Pb geochronology data from rock samples collected in the Dillon, Hamilton, Philipsburg, Townsend, and Wisdom 30′ x 60′ quadrangles, western Montana, 2020–2021: Montana Bureau of Mines and Geology Analytical Dataset 3.
Mosolf, J.G., and Sears, J., 2024, Geologic map of the Red Canyon 7.5′ quadrangle, Beaverhead and Madison counties, Montana: Montana Bureau of Mines and Geology Geologic Map 95, 1 sheet, scale 1:24,000.
Mosolf, J.G., Brennan, D.T., Elliott, C.G., Parker, S., and Salazar, R., in review, Major oxide and trace element analyses of rock samples collected in the Dillon and Wisdom 30′ x 60′ quadrangles, southwest Montana: Montana Bureau of Mines and Geology Analytical Dataset.
Okuma, A.F., 1971, Structure of the Southwestern Ruby Range near Dillon, MT: Harrisburg, State College, Pennsylvania State University, Ph.D. dissertation, 122 p.
Ostenaa, D., and Wood, C., 1990, Seismotectonic study for Clark Canyon Dam, Pick-Sloan Missouri Basin Program, Montana: U.S. Bureau of Reclamation Seismotectonic Report 90-4, 78 p., 1 pl.
Parker, S.D., and Gavillot, Y.G., 2024, Geologic map of the Laurin Canyon 7.5' quadrangle, Madison County, Montana: Montana Bureau of Mines and Geology Geologic Map 98, 1 sheet, scale 1:24,000.
Ruppel, E.T., O'Neill, J.M., and Lopez, D.A., 1993, Geologic map of the Dillon 1º x 2º quadrangle, Idaho and Montana: U.S. Geological Survey Miscellaneous Investigations Series Map I-1803-H, scale 1:250,000.
Schmid, R., Fettes, D., Harte, B., Davis E., and Desmons, J. A., 2007, Systematic nomenclature for metamorphic rocks: 1. How to name a metamorphic rock. Recommendations by the IUGS Subcommission on the Systematics of Metamorphic Rocks, available at https://www.bgs.ac.uk [Accessed March 2023].
Schmidt, C. J., and Garihan, J. M., 1983, Laramide tectonic development of the Rocky Mountain foreland of southwestern Montana, in Lowell, J.D. and Gries, R., eds.: Rocky Mountain foreland basins and uplifts: Rocky Mountain Association of Geologists, p. 271–294.
Stickney, M.C., and Bartholomew, M.J., 1987, Seismicity and late Quaternary faulting of the northern Basin and Range province, Montana and Idaho: Bulletin of the Seismological Society of America, v. 77, p. 1602–1625.
Stickney, M.C., Haller, K.M., and Machette, M.N., 2000, Quaternary faults and seismicity in Western Montana: Montana Bureau of Mines and Geology Special Publication 114, 1 sheet, scale 1:750,000.
Stotter, S.V., 2019, Determining the Precambrian structure and thermotectonic evolution of the central Ruby Range, southwest Montana: Missoula, University of Montana, M.S. thesis, 78 p.
Sun, S.S., and McDonough, W.F., 1989, Chemical and isotope systematics of oceanic basalts: Implications for mantle composition and processes, in Saunders, A.D., and Norry, M.J., eds., Magmatism in the ocean basins: Geological Society, London, Special Publications, v. 42, p. 313–345.
Thomas, R.C., and Sears, J.W., 2020, Middle Miocene through Pliocene sedimentation and tectonics in Montana: A record of the outbreak and passage of the Yellowstone Hotspot, in Metesh, J.J., and Vuke, S., eds.: Montana Bureau of Mines and Geology Special Publication 122: Geology of Montana—Geologic History, v. 1, 25 p., available at http://www.mbmg.mtech.edu/pubs/GeologyofMontana/
Tysdal, R.G., 1976, Geologic map of the northern part of Ruby Range, Madison County, Montana: U.S. Geological Survey, Miscellaneous Investigations Series Map I-951, scale 1:24,000.
Underwood, S.J., Childs, J.F., Walby, C.P., Lynn, H.B., Wall, Z.S., Cerino, M.T., and Bartlett, E., 2014, The Yellowstone and Regal talc mines and their geologic setting in southwestern Montana in Shaw, A., and Tikoff, B., Exploring the Northern Rocky Mountains: Geological Society of America Field Guide 37, p. 161–187, https://doi.org/10.1130/2014.0037(08).
Vuke, S.M., 2020, The Eocene through early Miocene sedimentary record in western Montana, in Metesh, J.J., and Vuke, S., eds.: Montana Bureau of Mines and Geology Special Publication 122: Geology of Montana—Geologic History, v. 1, 38 p., available at http://www.mbmg.mtech.edu/pubs/GeologyofMontana/
Vuke, S.M., Porter, K.W., Lonn, J.D., and Lopez, D.A., 2007, Geologic map of Montana: Montana Bureau of Mines and Geology Geologic Map 62, 73 p., 2 sheets, scale 1:500,000.
Wooden, J.L., Vitaliano, C.J., Koehler, S.W., and Ragland, P.C., 1978, The late Precambrian mafic dikes in the southern Tobacco Root Mountains, Montana: Geochemistry, Rb-Sr geochronology, and relationship to Belt tectonics: Canadian Journal of Earth Sciences, v. 15, p. 467–479.

ACKNOWLEDGMENTS

Amanda Rossi assisted field mapping and sample collection. Connie Thomson, Daniel Brennan, Stuart Parker, and Ray Salazar performed mineral separations at the MBMG Mineral Separation Laboratory. Andrew Kylander-Clark supported LA-ICPMS analyses and data reduction at the University of California, Santa Barbara. Ashley and Arron Steiner directed bulk-rock geochemical analyses at the Washington State University Peter Hooper Geoanalytical Laboratory. Yann Gavillot and Stuart Parker reviewed an early draft of the map report.

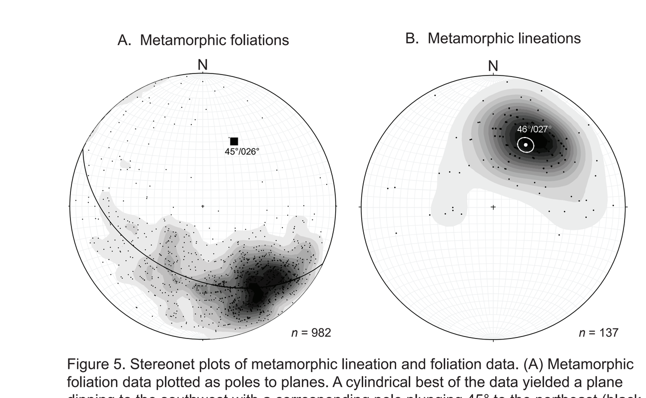

Figure 5. Stereonet plots of metamorphic lineation and foliation data. (A) Metamorphic foliation data plotted as poles to planes. A cylindrical best of the data yielded a plane dipping to the southwest with a corresponding pole plunging 45° to the northeast (black box), interpreted to be the general axis of folding in the map area. (B) Metamorphic lineation data. The mean vector is represented by a white circle plunging 46° to the northeast, similar to the fold axis in (A). The lineation and foliation data are plotted on lower-hemisphere projection, equal-area stereonets and fit with a Kamb contours.

Table 1. U-Pb zircon geochronology.

Sample	Lithology	Unit	Latitude (°N)	Longitude (°W)	# Spot analyses[a]	Method	Age (Ma)	2σ	MSWD[b]
KM20CR01	tuff	Tsc	45.1933	-112.4650	16/35	WM 206/238	10.5	0.1	2.1
JM23CR02	tuffaceous sandstone	Tsc	45.1933	-112.4646	26/120	MDA 206/238	10.7	0.1	1.6
JM23CR03	tourmaline granite	XAtp	45.1608	-112.4481	4/50	WM 207/206	1,882	47	2.6
JM23CR01	quartzofeldspathic gneiss	Adg	45.1617	-112.4031	30/60	MEA 207/206	2,772	23	6.1

Note. Zircon separates were prepared at MBMG and analyzed by LA-ICPMS at the University of California, Santa Barbara. Latitudes and longitudes are in the 1984 World Geodetic Survey (WGS84) datum. See Mosolf and Kylander-Clark (2023) and Brennan and others (in review) for full datasets and interpretations.
Method: MDA 206/238 — max depositional age, weighted mean of youngest $^{206}Pb/^{238}U$ dates
MEA 207/206 — minimum emplacement age determined by weighted mean of oldest $^{207}Pb/^{206}Pb$ dates
WM 206/238 — weighted mean of select $^{206}Pb/^{238}U$ dates interpreted to be emplacement age
[a]Numerator is the number of spots used for age calculation; the denominator is the total number of spots analyzed.
[b]MSWD is the Mean Square Weighted Deviation.

Geologic Map 110

Geologic Map of the Christensen Ranch 7.5′ Quadrangle, Southwestern Montana

Mapped and compiled by
Jesse G. Mosolf and Catherine McDonald

2025

https://doi.org/10.59691/GZLT6273

Research supported by the U.S. Geological Survey, National Cooperative Geologic Mapping Program, under USGS award G23AC00457.
GIS production: Jesse Mosolf, Patrick E. Gallagher, and Yiwen Li, MBMG. Map layout: Susan Smith, MBMG. Editing: Susan Barth, MBMG.